Rietveld refinement and diffuse phases transition of $Ba_{1-X}Bi_xTi_{0.8}Fe_{0.2}O_3$ ceramics at x=0.00, 0.05, 0.10 and 0.15 prepared by solid state method.

Najwa Gouitaa (najwa.gouitaa@gmail.com)
Universite Sidi Mohamed Ben Abdellah Faculte des Sciences et Techniques de Fes
LAMCHARFI Taj-dine
Universite Sidi Mohamed Ben Abdellah Faculte des Sciences et Techniques de Fes
Mfadal BOUAYAD
Universite Sidi Mohamed Ben Abdellah Faculte des Sciences et Techniques de Fes
ABDI Farid
Universite Sidi Mohamed Ben Abdellah Faculte des Sciences et Techniques de Fes
Mustapha Haddad
Universite Sidi Mohamed Ben Abdallah

Research Article

Keywords: Ba1-xBixTi0.80Fe0.20O3 ceramics, rietveld, structural, RAMAN spectra, dielectric properties, phase transition, Uchino, complex impedance

Posted Date: April 6th, 2020

DOI: https://doi.org/10.21203/rs.3.rs-21117/v1

Abstract

The effect of substitution of Baryum by Bismut in site A and titanium by iron in site A on structural, physical and electrical properties of $Ba_{1-x}Bi_xTi_{0.80}Fe_{0.20}O_3$ ceramics at (x=0.00, 0.05, 0.10 and 0.15) was investigated by X-ray diffraction, Scaning Electron Microscopy (SEM) as well as dielectric characterizations. The crystal phase was studied by using rietveld refinement. The result of rietveld refinement of X-ray powders diffraction of $Ba_{1-x}Bi_xTi_{0.80}Fe_{0.20}O_3$ shows that these compounds crystallize in tetragonal (P4mm) and hexagonal (P63mmc) for x=0.00 and 0.05 while at x=0.10 and 0.15 the hexagonal phase disappears and the tetragonal phase is stabilized. The structural parameters and the R-factors of these ceramics were succefully determined by the rietveld refinement. The Raman spectra confirms the disappearance of hexagonal phase in benefit of tetragonal phase as the Bi substitution increases. The dielectric measurements as function of temperature are studied and showed tree diffuse phase transitions transition from the ferroelectric rhombohedral phase to the ferroelectric orthorhombic T_{R-O} phase and the second one is from the ferroelectric orthorhombic phase to the ferroelectric T_{O-T} tetragonal phase. While the third one at high temperatures is the phase transition from the ferroelectric tetragonal phase to the paraelectric cubic phase T_m. These phases transition were displaced to the lower temperature with increasing of Bi substitution. And the value of dielectric permittivity increases gradually with increasing of Bi^{2+} contents. All these phase transitions showed a diffused phenomenon which can be well described by fitting the modified Ushino relation, $1/\varepsilon'_r = 1/\varepsilon'_{r,max}[1+((T-Tm)/2\delta)^{\gamma}]$. The complex impedance Cole–Cole plots showed negative temperature coefficient of resistivity (NTCR) behavior of the $Ba_{1-x}Bi_xTi_{0.80}Fe_{0.20}O_3$ for x=0.05 to 0.15 materials and decrease in grain and grain boundaries resistivity. The relaxation behavior in the test materials is found to be of Debye type.

Introduction

Multiferroic materials which combine simultaneously ferroelectricity and magnetic order are increasingly attracted the great attention of scientific community over the last decade because of interest in their potential applications in current and emerging technologies at information storage, MERAM, spintronics etc[1,2].

The tetragonal perovskite $BaTiO_3$ with a high dielectric constant, low dielectric loss, Curie temperature (T_c) of 120 °C and good piezoelectric, pyroelectric and ferroelectric properties[3] has been adapted as a popular candidate in the research of multiferroic materials. $BaTiO_3$ can act as a multiferroic material with the induction of ferromagnetism by doping transition metal (Mn, Fe, Co, Ni, Cr) ion[4,5]. The Fe doped $BaTiO_3$ has been reported to have magnetic ordering, where the Fe ions substitute into the Ti^{4+} sites[6,7]. It is observed that when Fe substituted at B-site, it improves the coercive field while at A-site substitution sample saturation magnetization increases[8]. However, the major problems of earlier BTFO ceramic are

the high Curie temperature which is displaced to the higher temperature with increasing of Fe doping contents[9] and the low dielectric constant which limited their application.

The co-substitution in $BaTiO_3$ ceramics opens new possibilities to improve physical properties. The effect of (Bi^{3+}, Li^{+}) and (La^{3+}, Na^{+}) co-substituted BT ceramics on structural, dielectric and ferroelectric properties were recently investigated[10,11]. And it has been reported that the substitution of Bi^{3+} ions into the Ba^{2+} sites ($Ba_{1-x}Bi_xTiO_3$) achieves a maximum dielectric constant at x = 0.05 [12]. The structure of $Ba_{1-x}Bi_xTiO_3$ ($x \leq 0.1$) was reported to be of a tetragonal phase [13, 14].

The present study is intended to study the influence of Bi doping on structural and dielectric properties of $Ba_{1-x}Bi_xTi_{0.80}Fe_{0.20}O_3$ solid solution at x = 0.0, 0.05, 0.10 and 0.15 Bi -doping concentration.

Experimental

The $Ba_{1-x}Bi_xTi_{0.80}Fe_{0.20}O_3$ ceramics at (x = 0.0, 0.05, 0.10 and 0.15) were prepared by the conventional solid-state method. The $BaCO_3$, Bi_2O_3, TiO_2 and Fe_2O_3 oxides were weighted in stoichiometric proportion and milled under acetone for 4 h. After that the powders were dried at 80 °C for 24 h. The dried powders were grinded using agate mortar for 30 min and then calcineted in air at 1100 °C for 4 h. The crystal structure of the product ($Ba_{1-x}Bi_xTi_{0.80}Fe_{0.20}O_3$) was characterized by X-ray diffraction (XPERT-PRO with Cu Kα radiation with λ = 1.5406 Å). And the refinements were carried out using FULLPROF program based on Rietveld method. The profile refinement parameters included a scale factor, pseudo-Voigt peak. The background was refined to a six-degree polynomial. And the lattice parameters, unit cell volume, and the statistical parameters such as: R_p, R_{wp} and χ^2 were obtained using Fullprof refinement software. The structure was confirmed by Raman spectroscopy at room temperature.

The calcined powders were pressed into pellets, after adding few drops of 1 wt% Polyvinyl Alcohol (PVA) as a binder, and sintered in air at 1200 °C for 6 h. The grain size and the micromorphology of the pellets were detected on a fracture of surface by a scanning electron microscope (SEM). And the dielectric properties as function of frequency and temperature were studied with Agilent E4980A (20 Hz-2 MHz). After that we have tested the electrical properties by measuring the complex impedance as function of frequency.

Results And Discussion

X-ray diffraction results

The effect of Bi substitution on the structural properties (DRX) of the $BaTi_{0.80}Fe_{0.20}O_3$ (BTFO) product was studied for the percentages of (x = 0.00, 0.05, 0.10 and 0.15). The Fig. 1.a. shows the XRD patterns of these products. The coexistence of the characteristic peaks of the two hexagonal and tetragonal phases is clear for x = 0.00 (BTFO) and x = 0.05. Whereas for x = 0.10 and 0.15, the hexagonal phase disappears

completely and the peaks of the tetragonal phase dominate. To better see the effect of Bi on the evolution of the BTFO structure, we zoomed on the two most intense peaks (101) of the tetragonal phase and (104) of the hexagonal phase (Fig. 1. b). We note that the intensity of the peak (104) decreases tofrom x = 0.0 to x = 0.05 and then disappears beyond this percentage. And the peak (101) of the tetragonal phase becomes stable beyond 0.05 of Bi and moves towards the lower angles for x = 0.05 and then towards the high angles at x = 0.10 and 0.15, which indicates the incorporation of Bi into the BTFO ceramic.

The fitting of these phases by using the rietveld refinement method is shown in Fig. 2 and indicate that all the diffraction peaks are indexed with the coexistence of tetragonal and hexagonal phase at x = 0.00 and 0.05 of prepared samples. While at x = 0.10 and 0.15 only the tetragonal phase is identified. The tetragonal phase becomes predominant with increasing of Bi contents and stabilizes at percentage higher than 0.10 of Bi substitution. This suggests that the concentration higher than 0.10 of Bi enhances the hexagonal phase formation. Thus, the structure of the present ceramics change from P63/mmc to P4mm with increasing x from 0.00 to 0.15 and there is no obvious secondary phase observed. These results of refinement confirm the XRD patterns observation.

The rietveld adjustment allowed us to determine the structural parameters of $Ba_{1-x}Bi_xTi_{0.8}Fe_{0.2}O_3$ ceramics for x = 0.00, 0.05, 0.10 and 0.15, ie the R-factors (R_p, R_{wp} and χ^2), cell parameters and volume (see Table 1). According to these values we find that R < 15.0 and χ^2 < 2.0, for the tetragonal phase, which indicates a better refinement of the powders[15]. The parameters of unit cell a, c and the tetragonality c / a are plotted on the Fig. 3, one notices that c/a decreases for x = 0.05 accompanied by a decrease of ‘a’ parameter due to the dominance Fe^{3+} ions with ionic radius (r_i (Fe^{3+}) = 0.645 Å) greater than the ionic radius, of the substituted Ti^{4+} ion (r_i (Ti^{4+}) = 0.605 Å). Whereas above this concentration of x = 0.05, when the hexagonal phase completely disappears, c/a increases almost linearly. This is probably due to the substitution of Bi^{3+} ion with (r_i (Bi^{3+}) = 1.2 Å) smaller than that of the substituted ion (r_i (Ba^{2+}) = 1.35 Å). It should be noted that this evolution, produced by the solid solution, is not only due to the substitution of a small ion to a larger one, but also to the creation of oxygen vacancies[15].

The phase composition of crystallized powders was studied by Raman spectroscopy, a highly sensitive spectroscopic technique for probing the local structure of atoms. The Raman spectra of $Ba_{1-x}Bi_xTi_{0.80}Fe_{0.20}O_3$ for x = 0.00, 0.05, 0.10 and 0.15 are shown in Fig. 4. For x = 0.00, the spectra have seven bands at 120, 184, 248, 350, 500, 680, 880 cm^{-1} related to the modes A1g, E1g, E1g, E2g, A1g, A1g and A1g respectively, characteristic of the hexagonal phase[16] of BTFO. The band around 680 cm^{-1} is related to Fe^{3+}. Thus, it is possible to prove by Raman spectroscopy that the developed ceramic has a hexagonal phase. These results are consistent with those of the literature for iron-doped $BaTiO_3$. By substituting BTFO by Bi, five peaks are observed at 178, 300, 504, 624 and 710 cm^{-1}, which correspond well to the tetragonal phase[17,18]. The band at 305 cm^{-1}, attributed to B1 + E (LO + TO), is characteristic of the tetragonal phase. The intensity of this band and the A1 band at 178 cm^{-1} increases gradually, indicating an increase in tetragonality, which is in good agreement with the XRD. An offset of the position of the

band between 710 and 720 cm^{-1} was observed. We propose that doping with Bi^{3+} ions induces the valence change of Fe ions from high to low values to maintain the neutrality of the charge. Since the ionic radius of Fe^{2+} (0.76 Å) is greater than that of Fe^{3+} (0.645 Å) and Fe^{4+} (0.585 Å), the Fe - O bonds have a higher covalence so that the 710 cm^{-1} band shifted to the higher frequency. In addition, the peak A_{1g} at 680 cm^{-1}, characteristic of the hexagonal phase, shifts widely and decreases in intensity with Bi substitution for x = 0.05 and finally disappears at x = 0.10 and 0.15. This indicates the disappearance of the hexagonal phase at these levels of Bi.

The Fig. 5 shows the SEM micrographs of $Ba_{1-x}Bi_xTi_{0.80}Fe_{0.20}O_3$ ceramics for x = 0.00, 0.05, 0.10 and 0.15 sintered at 1200 °C for 6 hours. These images exhibit fine grains with different grains size. The size distribution of the formed grains is found to be non-uniform. The irregular morphology with various sizes of the grains is clearly noticeable in sample with x = 0.00, which shows the coexistence of smaller grains with larger ones.

The average grains size is found to be 1.478 µm, 1.896µ m, 1.990µ m and 3.188µ m, respectively, for x = 0.00, 0.05, 0.10 and 0.15. It is clear that the average grain size increases with increase of Bi content (Fig. 6). The grain form became more homogeneous with doping of Bi at x = 0.15 comparing with the others samples which grain forms are inhomogeneous especially at x = 0.00. Furthermore, the sample with x = 0.00 and 0.05 of Bi have different grains forms which may be reflect the coexistence of two phase in these materials. While at x = 0.10 and 0.15 the tetragonal grain form is clearly observed. These results were consistent with the DRX results

x	**0.00**		**0.05**		**0.10 0.10**	**0.15**
Statistical parameters	Tetragonal R_p= 6.39 R_{wp}=8.54 χ^2 = 1	Hexagonal R_p= 8.31 R_{wp}=13.40 χ^2 = 3.90	Tetragonal R_p= 5.96 R_{wp}=7.53 χ^2 = 1.34	Hexagonal R_p= 7.55 R_{wp}=11.4 χ^2 = 3.54	Tetragonal R_p= 4.78 R_{wp}=6.11 χ^2 = 0.960	Tetragonal R_p= 6.71 R_{wp}= 8.66 χ^2 = 1.56
Bragg R-factor	55.13	36.02	36.5	40.6	21.8	14.6
Lattice constants (Å)	a = b = 4.00668 c = 4.03009	a = b = 5.839 c = 13.7607	a = b = 4.00524 c = 4.01916	a = b = 5.654 c = 13.423	a = b = 4.004677 c = 4.05988	a = b = 4.005567 c = 4.081004
Volume (Å ^{3})	64.697	406.309	64.475	420.19	63.54	62.86
Space group	P4mm	P 63/mmc	P4 m	P63/mmc	P4mm	P4mm

Dielectric properties

The Fig. 7 displays the evolution of the real part of the dielectric permittivity (ε'_r) as a function of temperature (from R.T to 450 °C) at various frequencies (from 5 KHz to 2 MHz). There are tree dielectric

anomalies. The first anomaly corresponds to the phase transition from the ferroelectric rhombohedral phase to the ferroelectric orthorhombic T_{R-O} phase. It is present for all ceramics at different temperatures. The second anomaly corresponds to the phase transition from the ferroelectric orthorhombic phase to the ferroelectric T_{O-T} tetragonal phase. While the third anomaly at high temperatures is the phase transition from the ferroelectric tetragonal phase to the paraelectric cubic phase T_m [19]. These tree peaks are due to different phase transitions of $BiFeO_3$ and $BaTiO_3$[20].

The evolution of the maximum dielectric permittivity and temperature of the three phase transitions at a frequency of 5 KHz was also studied. It appears from the Fig. 8.a that the dielectric constant of BBTFO ceramics increases significantly with Bi doping for all phase transitions. This could be due to the role of conductive bismuth ions in the $BaTiO_3$ network substituted the barium ions[21]. In addition, the Bi^{3+} ion substitutes Ba^{2+} for $BaTiO_3$, so that the ionic volume of site A decreases due to vacancy of the barium, creating a larger active space for Ti^{4+}. From the + 2 to + 3 increase in the ion of A site, a residual positive charge appears and the mutual effect between sites A and B (Ti^{4+}) becomes stronger. Thus, the polarization of Ti^{4+} is improved, then the dielectric constant increases strongly[22]. This increase in ε'_r 'with the increase in Bi is also found by S. Islam et al[23], for the $BaTiO_3$ ceramics substituted for Bi, but the values of ε'_r that they obtained are greater than our values due to the Fe co-substitution.

The decrease of T_m (Fig. 8.b) with Bi doping indicates a partial substitution of Ba^{2+} ions by Bi^{3+} in the perovskite network. These results are in good agreement with those found by S. Islam et al[23]. Thus, the advantage of the co-substitution of BTF by the ions of Bi in site A is the maximization of the value of the dielectric permittivity and the minimization of the phase transition temperature.

All the present phase transitions present a clear diffuse behavior. To explain this type of behavior (ferroelectric with diffuse phase transition) the diffuseness character of the phase transition or the diffuseness coefficient (γ) was obtained by fitting the dielectric constant curves with the modified Uchino's phase transition as given below[24]:

$$1/\varepsilon'_r = 1/\varepsilon'_{r,max}\left[1+\left(\frac{(T-Tm)}{2\delta}\right)^{\gamma}\right]$$

This equation may be written as the following:

$$\mathbf{Ln\left[\left(\left(\varepsilon'_{r,max}/\varepsilon'_r\right)-1\right)\right] = \gamma\, ln\,(T-T_m) - \gamma\, ln 2\delta}$$

Where T_m is the temperature corresponding to the maximum of dielectric constant, $\varepsilon'_{r,max}$ is the permittivity at T_m, γ is the degree of dielectric relaxation. It value is 1 for normal ferroelectrics following CurieeWeiss law, 2 for ideal relaxor ferroelectrics. In general γ takes a value between these limits ($1 < \gamma < 2$) indicating an incomplete diffuse phase transition. The value of δ represents the degree of diffuseness for

transition peaks. Linear relationships are observed in the plot of ln (($\varepsilon'_{r,max}$ / ε'_r)-1) versus ln (T-T_m) at 5 KHz frequency for all the samples as it is shown in Figs. 9, 10 and 11. By fitting the experimental data to the modified Uchino equation, We notice that certain values of the diffusivity parameter γ are close to 1 (table.2) but the transition always remains diffuse and relaxor behevior, this is can be explained by the large values of δ. The other values of γ between 1.49 and 2 indicate that the type of the transition is relatively diffuse and present a relaxor behavior. On the other hand, the values of "γ" greater than 2 or very less than 1, the distribution of the phase temperatures of these ceramics is no longer a Gaussian as it was described by Smolenski[25] which limits the validity of the Uchino's law of these compounds.

The diffusion factor δ (table.2) is maximum for x = 0.05 for the three phase transitions then decreases to x = 0.10 and thereafter increases to x = 0.15 of Bi. The maximum value of δ shows that the three phase transitions are very diffuse at x = 0.05, while they are less diffuse at x = 0.10.

The diffuse phase transition behavior observed in these ceramics can be induced by many reasons, such as the fluctuation of the microscopic composition, the melting of micropolar regions in macropolar regions or a coupling of the parameter order and local disorder generated by a local constraint. The disorder of the structure of the ceramics of $Ba_{1-x}Bi_xTi_{0.80}Fe_{0.20}O_3$ may result from a substitution of two ions Bi^{3+} and Fe^{3+} in the two crystallographic sites Ba^{2+} and Ti^{4+} respectively, thus leading to nanometric heterogeneity in the compounds and consequently to a distribution of various local Curie points[26,27], then to a random distribution of the electric strain field in mixed oxide compounds which is the main reason leading to diffusion behavior as reported by Vugmeister[28].

Table.2. Refined structural parameters of $Ba_{1-x}Bi_xTi_{0.80}Fe_{0.20}O_3$ ceramics for x = 0.00, 0.05, 0.10 and 0.15.

Phase transition	x	0.00	0.05	0.10	0.15
T_{R-O}	δ	----	86.17	29.22	56.7
	γ	----	1.49	2	2.00
T_{O-T}	δ	----	----	22.9	61
	γ	----	----	2.28	1.99
T_m	δ	----	323	12.18	82.82
	γ	----	1.08	1.62	1.01

Dielectric constant as function of frequency: The Fig. 12 illustrates the real part of the dielectric constant (ε'_r) as a function of frequency of $Ba_{1-x}Bi_xTi_{0.80}Fe_{0.20}O_3$ ceramics at x = 0.00, 0.05, 0.10 and 0.15 sintered at 1200 °C/6 h. All the compositions have higher values of the dielectric constant at low frequencies. The permittivity decreases gradually with increasing frequency and becomes constant at very high frequency. Such frequency-dependent dielectric behavior can be explained by Koops's theory which depends on the Maxwell Wagner model for non-homogeneous crystal structure[29–31]. This model

suggests that a typical dielectric ceramic is composed of well conductive grains usually separated by resistive grain boundaries (low conductive). When an external electric field is applied to a dielectric ceramic, the charge carriers begin to migrate through the conductive grain and pile up at the boundaries of the resistive grain. As a result, a strong polarization (spatial charge polarization) occurs in the dielectric ceramic, resulting in high dielectric permittivity. In this case, the low-conductive grain boundaries contribute to the higher value of the permittivity at a lower frequency. Different types of polarization mechanisms are also responsible for the higher values of the permittivity in the low frequency region. Indeed, in the low frequency region, the four polarization mechanisms (ionic, electronic, dipolar polarization and space charge) contribute to the total polarization of the compound, which is responsible of a high dielectric permittivity. But with the increase of the frequency (i.e. in the high frequency region), the contribution of some of the polarization mechanisms to the total one is interrupted which results in lower permittivity values.

Electric properties

To understand the high-temperature dielectric dispersion, the complex Cole–Cole equation was used to analyze the impedance data. The Fig. 10 shows the complex impedance spectrum plots of $Ba_{1-x}Bi_xTi_{0.80}Fe_{0.20}O_3$ ceramics for x = 0.05 at different measurement temperature from 100 °C to 400 °C. The feature of impedance spectra is almost similar at different temperatures. However all the curves showed a tendency to bend towards the abscissa to form semicircles with their centers on the real axis, having comparatively larger radius showing an ideal Debye type behavior[32,33]. The radius of curvature of the arcs decreases with increasing temperature, which reveals that the conductivity of the sample increases as temperature increases and indicate also a negative temperature coefficient of resistivity (NTCR) behavior of the test materials[34,35]

According to the impedance spectrum data obtained of $Ba_{1-x}Bi_xTi_{0.80}Fe_{0.20}O_3$ ceramics at x = 0.00, 0.05, 0.10 and 0.15 at 400 °C of measurement temperature (Fig. 11) the Complex impedance spectrum of all the samples shows the presence of an arc of a circle with the center below the real axis indicating the contribution of both ceramic's boundaries and grain boundaries [36].

The electrical equivalent circuit corresponding to the sample impedance response is shown as inset of Fig. 11 and is represented by a number of elements, one R/C and other R/CPE connected in series. The values of resistance of both grain and grains boundaries are given by the fitting of the test materials by using the equivalent circuit plots. The Fig. 12 shows that the grains and grain boundaries resistivity increase with increasing of Bi contents from 0.00 to 0.05 indicating a positive temperature coefficient of resistivity (PTCR). While these resistivities decrease from x = 0.05 to 0.15 of Bi substitution showing a negative temperature coefficient of resistivity (NTCR).

Conclusion

In this study the effect of Bi substitution on structural and dielectric properties of $BaTi_{0.80}Fe_{0.20}O_3$ ceramics at x = 0.00, 0.05, 0.10 and 0.15 was studied. The rietveld refinement showed the formation of

tetragonal and hexagonal phase for x = 0.00 and 0.05 while only the tetragonal phase is clearly observed for x = 0.10 and 0.15. The dielectric measurement showed the existence of tree phase transitions. The temperature corresponding to these phase transition shifted to lower temperature with increase of Bi substitution. The diffuseness character is defined by modified Ushino law and indicates that the diffusivity γ corresponds to a very broad relaxation and a higher disorder in all the samples. The complex impedance spectroscopy approved the grain and grain boundary contributions towards electrical conductivity and the presence of Debye type of relaxation in the materials.

References

1. F. Wang, J.-M. Liu and Z.F. Ren, Adv. Phys. 58 (**2009**) 321.
2. H. Chi, C.J. Xiao, S.M. Feng, F.Y. Li, C.Q. Jin, X.H. Wang, R.Z. Chen and L.T. Li, J. Appl. Phys. 98 (**2005**). Paper No. 103519.
3. Pradhan, G. Roy. Researcher, 5 (3) (**2013**), pp. 63-67
4. Guo, L. Pan, C. Bi, H. Qiu, X. Zhao, L. Yang, M.Y. Rafique. J. Magn. Magn. Mater., 325 (**2013**), pp. 24-28
5. Nakayama and H. Katayama-Yoshida. J. Appl. Phys., 40 (**2001**), p. L1355.
6. Y. Qiu, W. Li, Y. Liu, G.H. Liu, Y.Q. Wu, N. Chen, Trans. Nonferrous Met. Soc. China 20 (**2010**) 1911.
7. P. Du, Z.J. Hu, Q.F. Han, X.M. Qin, W.Z. Shi, J. Alloys Compd. 492 (**2010**) L79.
8. Maikhuri, A.K. Panwar and A. Jha. J. Appl. Phys., 113 (**2013**), p. 17D915.
9. N. Apostolova, A. T. Apostolov, Safa Golrokh Bahoosh and Julia M. Wesselinowa. JOURNAL OF APPLIED PHYSICS 113, 203904 (**2013**).
10. S. Alkathy, K.C. Kiran, K. Bokinala, K. C. James Raju. ceramics. J. Mater. Sci. Mater. Electron., 27 (**2016**), pp. 3175-3181
11. S.Alkathy, K.C. James Raju. J. Alloys Compd., 737 (**2018**), pp. 464-476.
12. P. Jiang, M. Zeng, K.W. Kowk, H.L.W. Chan, Key Eng. Mater. 334 (**2007**) 977.
13. Widi Yansen, Kadek Juliana Parwanta, Hadiyawarman, Deokhyeon Kim, Younmi Gwan, Jaeyeong Kim, Chunli Liu, Chang Uk Jung, Bo Wha Lee, J. Korean. Phys. Soc. 63 (3) (**2013**) 306.
14. Vittayakorn, J. Appl. Sci. Res. 2 (12) (**2006**) 1319.
15. R. Das, R.N.P. Choudhary, B.K. Samantray. Mater Chem Phys, 101, pp. 228-233, (**2007)**.
16. Murugesan, R. Nithya and S. Kalainathan, Int. J. ChemTech Res., 6, 1633 (**2014**).
17. Eror N.G. Loehr T.M, Cornilsen B.C. Ferroelectrics **1980**, 28, 321–324.
18. Venkateswaran, U.D.; Naik, V.M.; Naik, R. Phys. Rev. B **1998**, 58, 14256–14260.
19. Poonam Kumari, Radheshyam Rai, Seema Sharma and M. A. Valente. JOURNAL OF ADVANCED DIELECTRICS. Vol. 7, No. 5 (**2017**) 1750034 (10 pages).
20. Fayçal Bourguiba, Ah. Dhahri, Tarek Tahri, J. Dhahri, N. Abdelmoula, K. Taibi, E.K. Hlil. Journal of Alloys and Compounds 675 (**2016**) 174e182.

21. Moganti Venkata Someswara Rao, Kocharlakota Venkata Ramesh, Majeti Naga Venkata Ramesh, BonthulaSrinivasa Rao. Advances in Materials Physics and Chemistry, 3, 77-82, **2013**.
22. Thirumalai, B. P. Shanmugavel. Journal of Microwave Power and Electromagnetic Energy, 45 (3), pp. 121-127, **2011**.
23. Islam, A. Siddika, N. A Ahmed, N. Khatun, S. N. Rahman. AIJRSTEM 15-814; **2015**.
24. S. Echatoui, T. Lamcharfi, S. Sayouri, L. Hajji, A. Alimoussa, Phys. Chem. News, 26 (**2005**) 40-46.
25. A. Smolensky, V.A. Isupov, A.I. Agranovskaya and S.N. Propov, Soviet. Phys. Solid State, 2, 2584, **1961**.
26. M. Pilgrim, A.E. Sutherland, S.R. Winzer. J. Am. Ceram. Soc. 73(10), 3122– 3135, **1990**.
27. M. Bobade, D.D. Gulwade, A.R. Kulkarni, P. Gopalan. J. Appl. Phys. 97, 074105, **2005**.
28. E. Vugmeister, M.D. Glinchuk. Rev. Mod. Phys. 62, 993, **1990**.
29. G. Koops. Physical Review 83.1: 121, **1951**.
30. C. Maxwell, Electricity and Magnetism . Oxford University Press, London, **1973**.
31. Wagner, Karl Willy. Annalen der Physik 345.5: 817-855, **1913**.
32. Khelifi, I.Zouari, A. Al-Hajry, N. Abdelmoula, D. Mezzane, H. Khemakhem. Ceramics International 41(**2015**)12958– 12966.
33. Gouitaa, T.Lamcharfi, Mf.Bouayad, F.Abdi, N.Hadi. Journal of Materials Science: Materials in Electronics, DOI 10.1007/s10854-018-8666-3, **2018**.
34. Ouyang, H. Zhang, D.Xue, Z.Li. Journal of Materials Science: Materials in Electronics. October **2013**, Volume 24, Issue 10, pp 3932–3939.
35. Xue, H. Zhang, Y. Li, Y. Liu and Z. Li. Journal of Materials Science: Materials in Electronics. July **2012**, Volume 23, Issue 7, pp 1306–1312.
36. D. Li, C. D. Feng, and P. H. Xiang. Electrical. Jpn. J. Appl. Phys., vol.42, pp.7387 7391, **2003**.

Figures

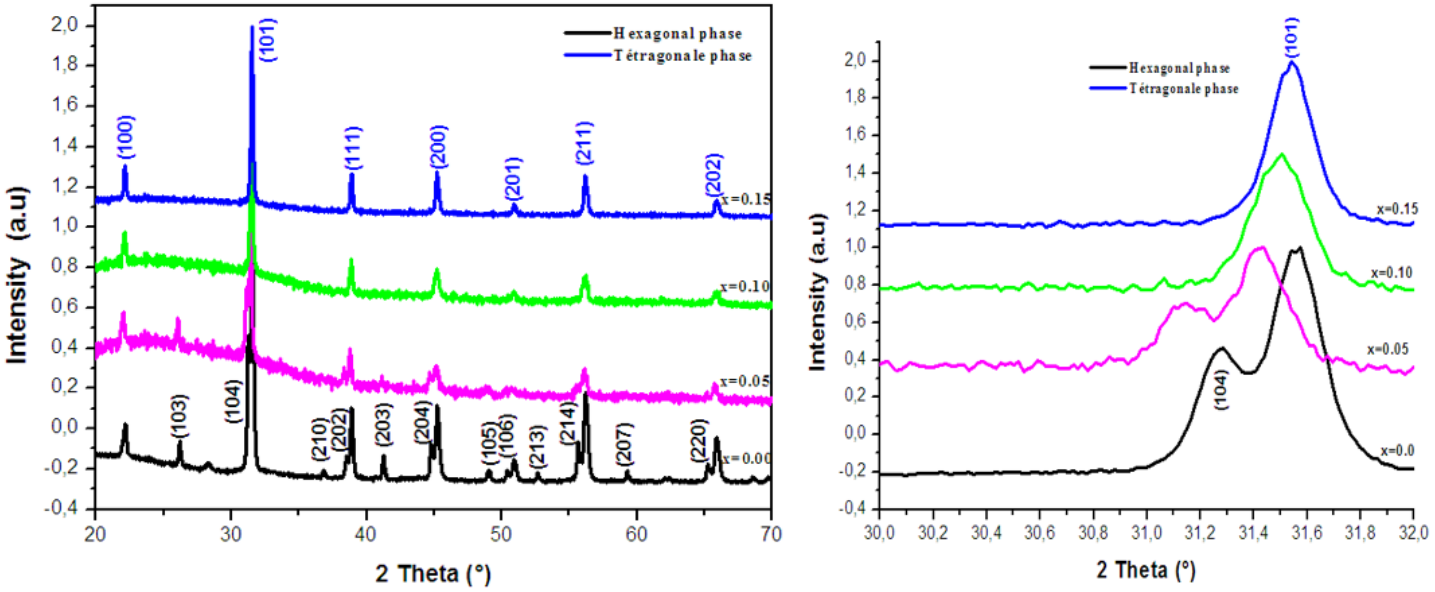

Figure 1

a. XRD patterns of Ba1-xBixTi0.80Fe0.20O3 ceramics for x=0.00, 0.05, 0.10 and 0.15. b. (101) and (104) peaks of Ba1-xBixTi0.80Fe0.20O3 ceramics for x=0.00, 0.05, 0.10 and 0.15.

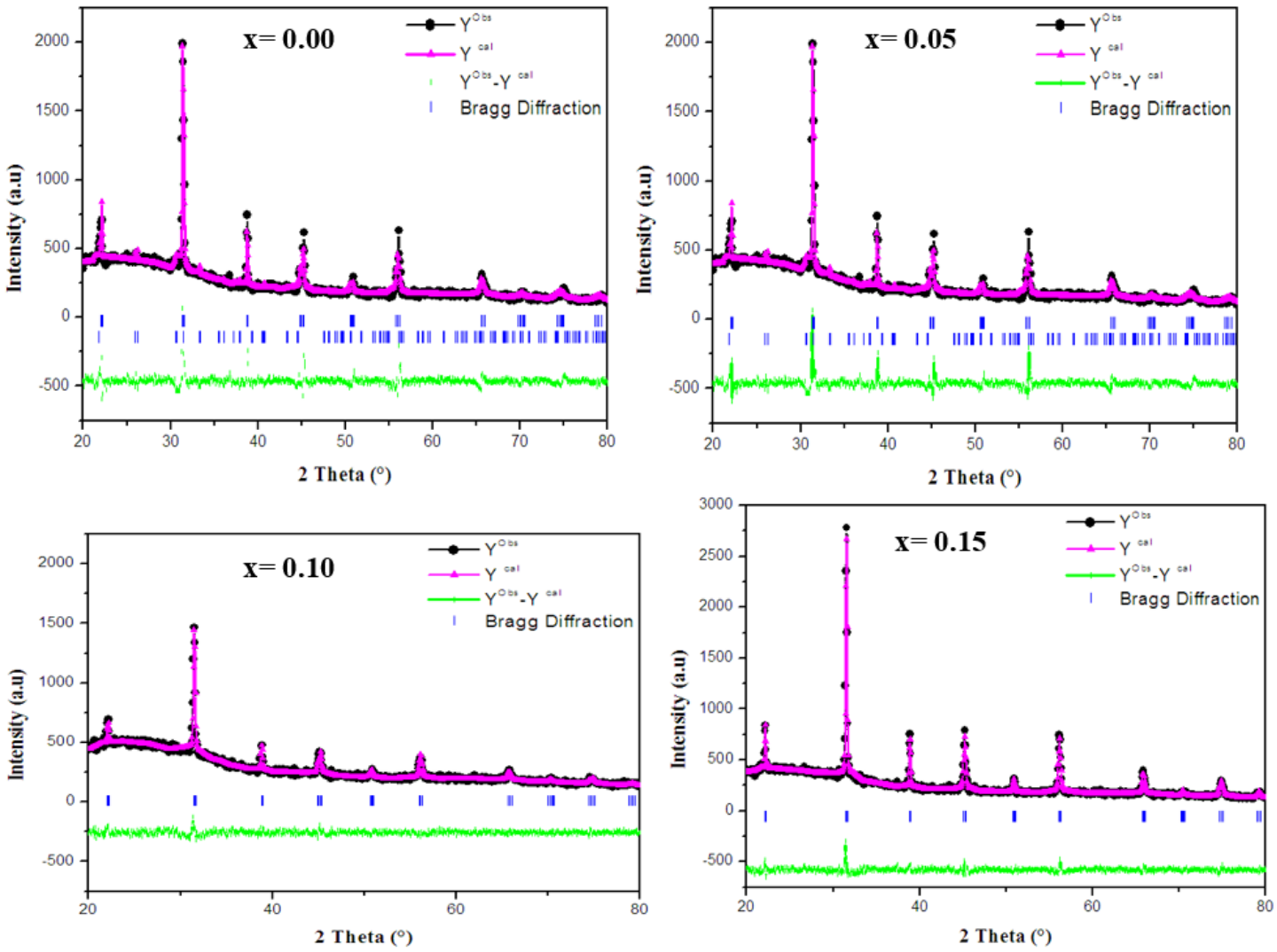

Figure 2

Rietveld plots of XRD data for Ba1-xBixTi0.80Fe0.20O3 ceramics. The points are the observed profile while the solid line is the calculated profile. Positions for the Bragg reflection are marked by vertical bras. The line curve at the bottom of the diagram gives the difference between observed and calculated profiles.

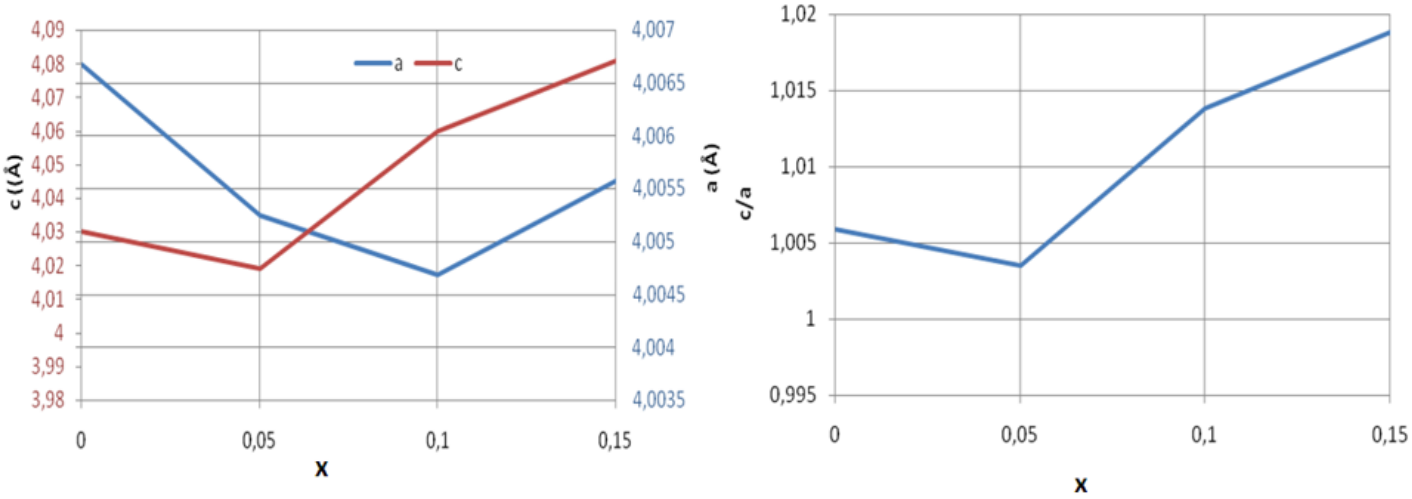

Figure 3

Evolution of a, c and c/a of Ba1-xBixTi0.80Fe0.20O3 ceramics as function of Bi substitution from x=0.00 to 0.15.

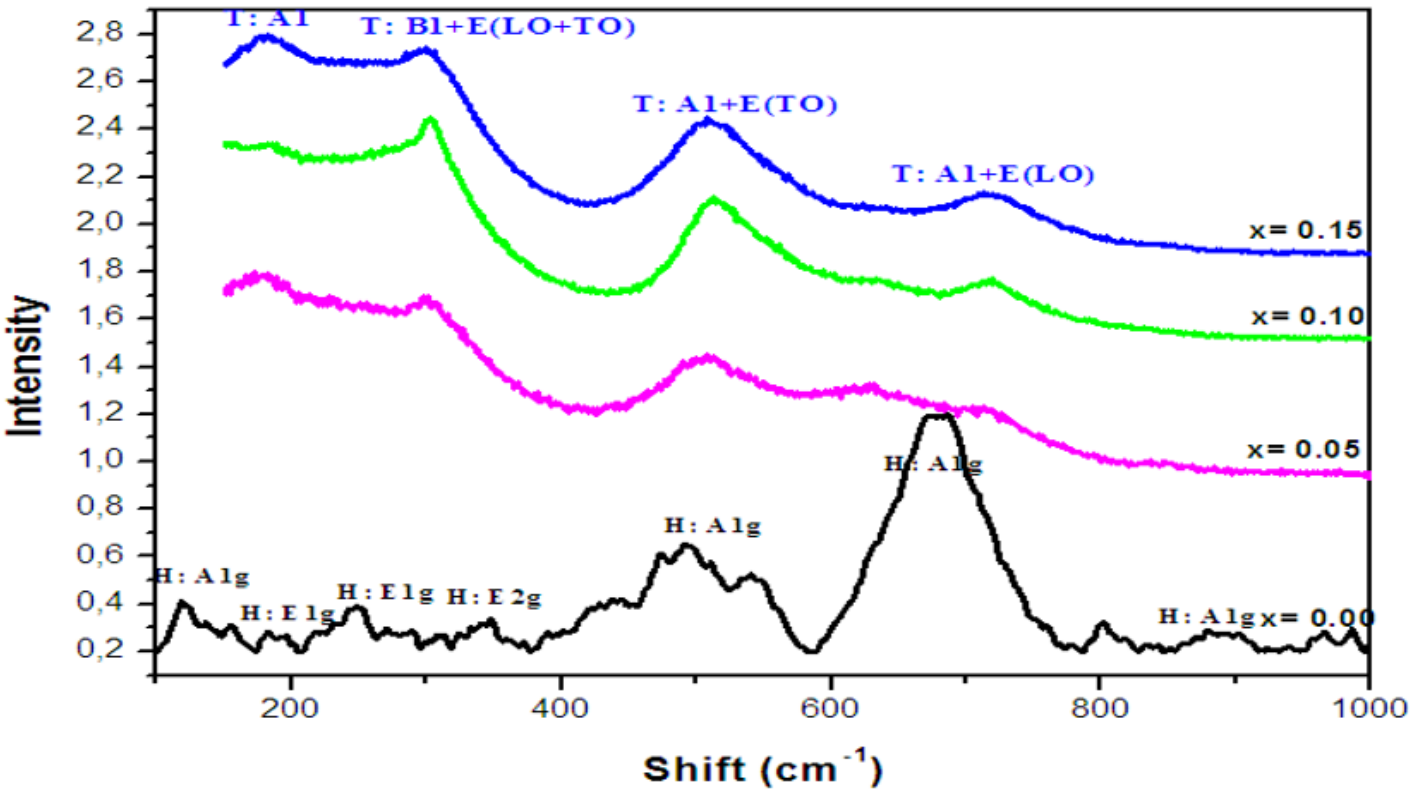

Figure 4

Raman spectra of Ba1-xBixTi0.80Fe0.20O3 ceramics at different substitution concentrations measured at room temperature.

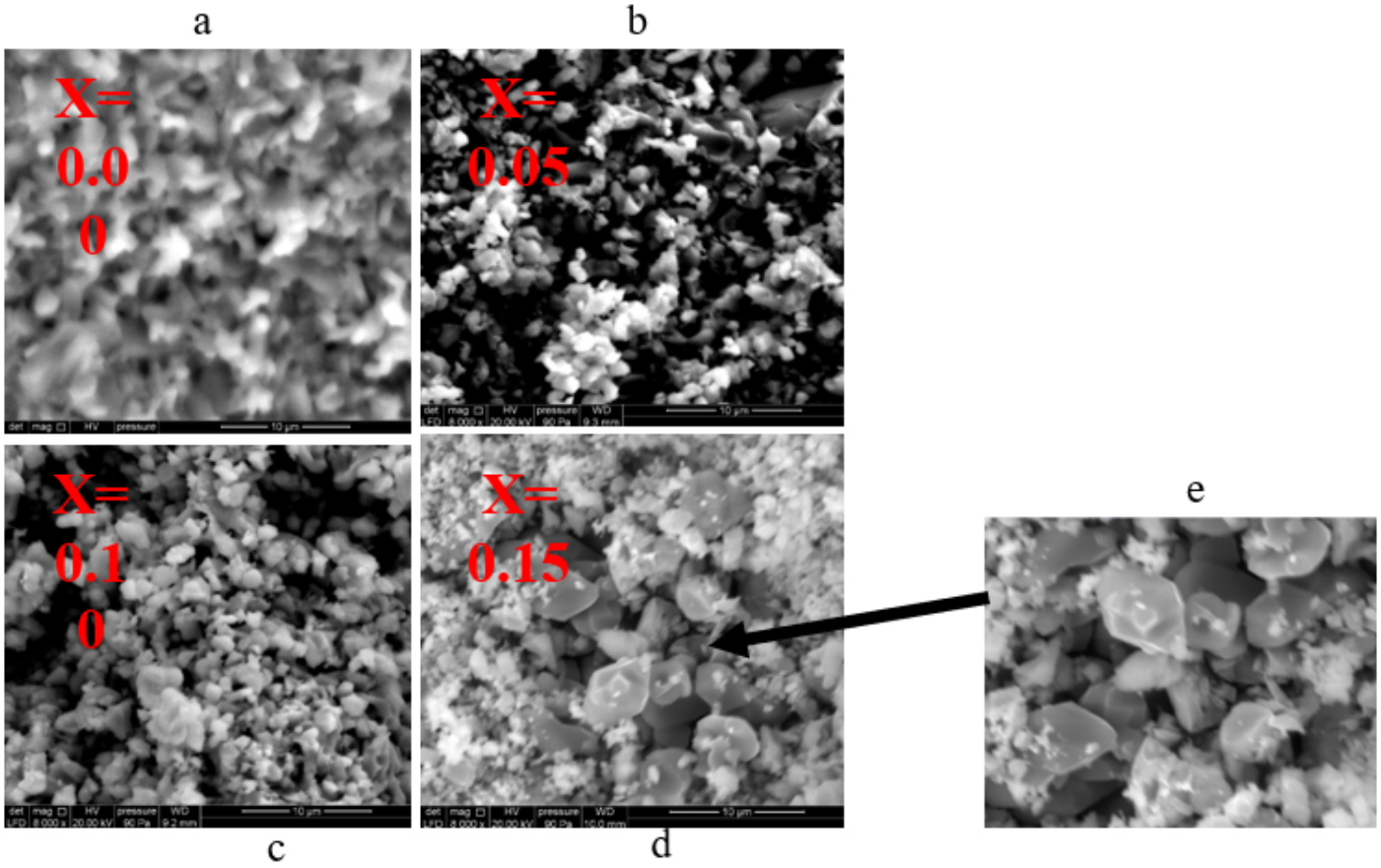

Figure 5

SEM micrographs of Ba1-xBixTi0.80Fe0.20O3 ceramics x= a. 0.00, b. 0.05, c. 0.10 and d. 0.15. e. Zoom on the composition with x=0.15 of Bi (picture d).

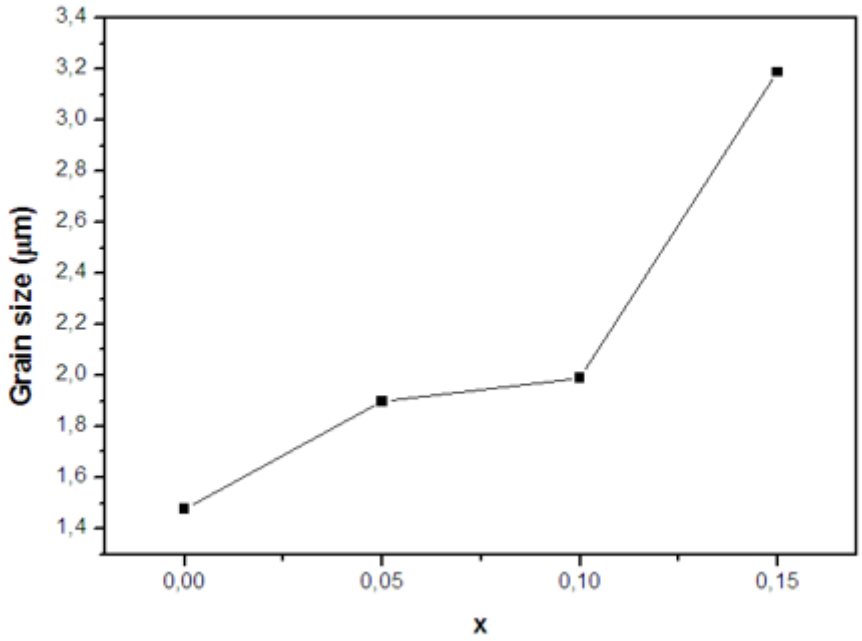

Figure 6

Grain size evolution of Ba1-xBixTi0.80Fe0.20O3 ceramics as function of Bi substitution from x=0.00 to 0.15.

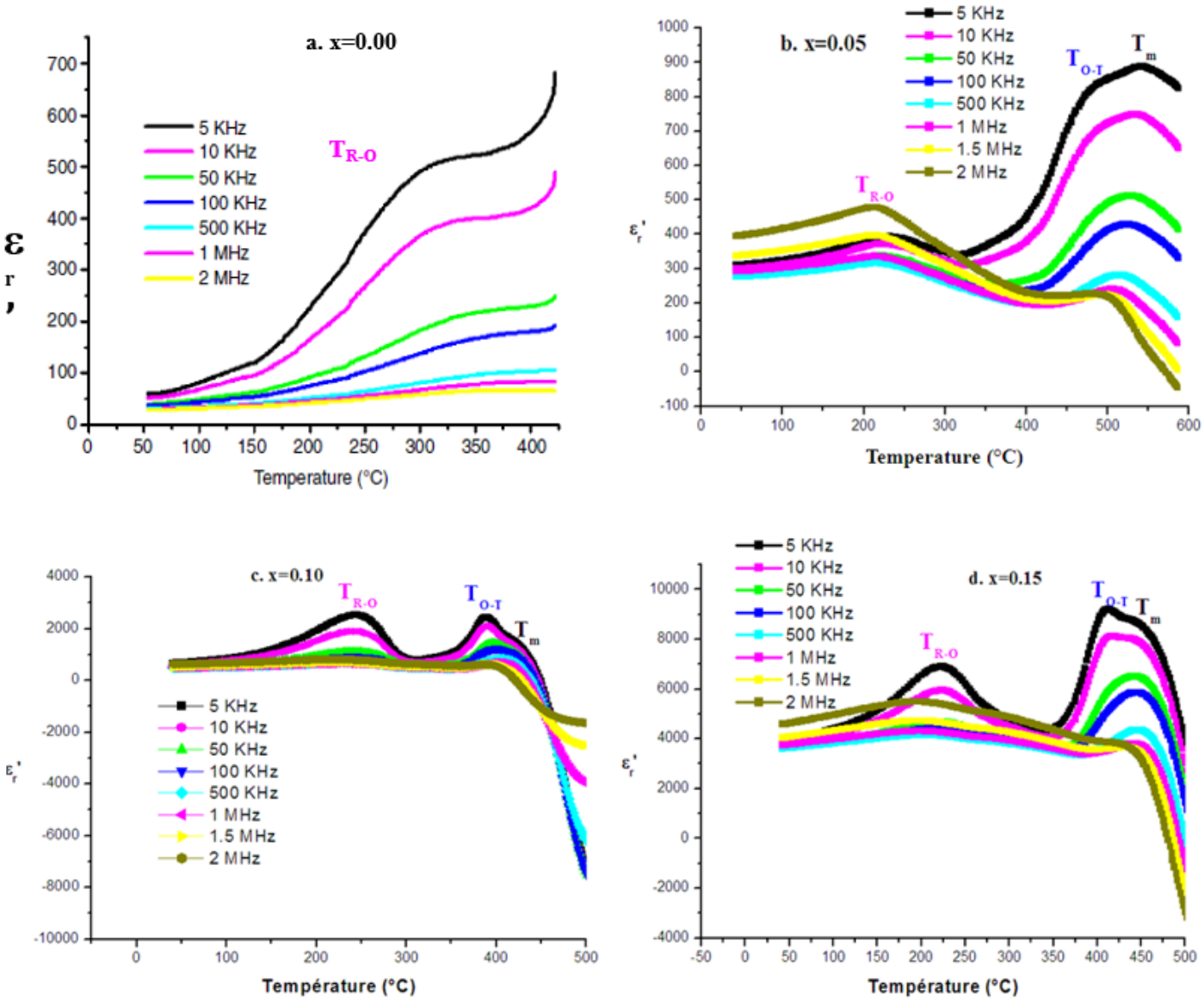

Figure 7

Dielectric constant dependent temperature at different frequencies of Ba1-xBixTi0.80Fe0.20O3ceramics for x= 0.00, 0.05, 0.10 and 0.15.

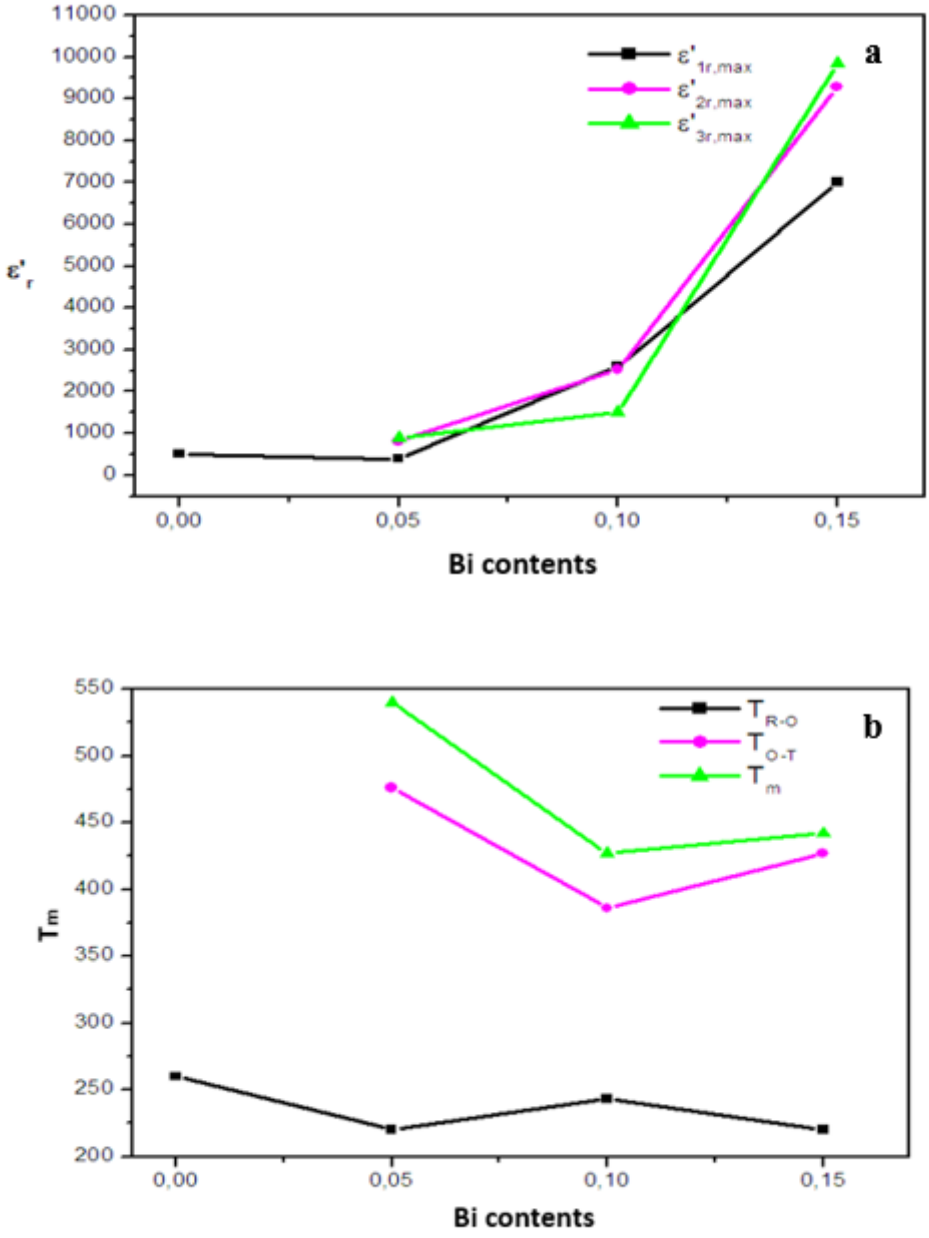

Figure 8

Evolution of maximum of dielectric constant and temperature as function of Bi contents from x=0.00 to 0.15 of a. TR-O, b. TO-T and c. Tm

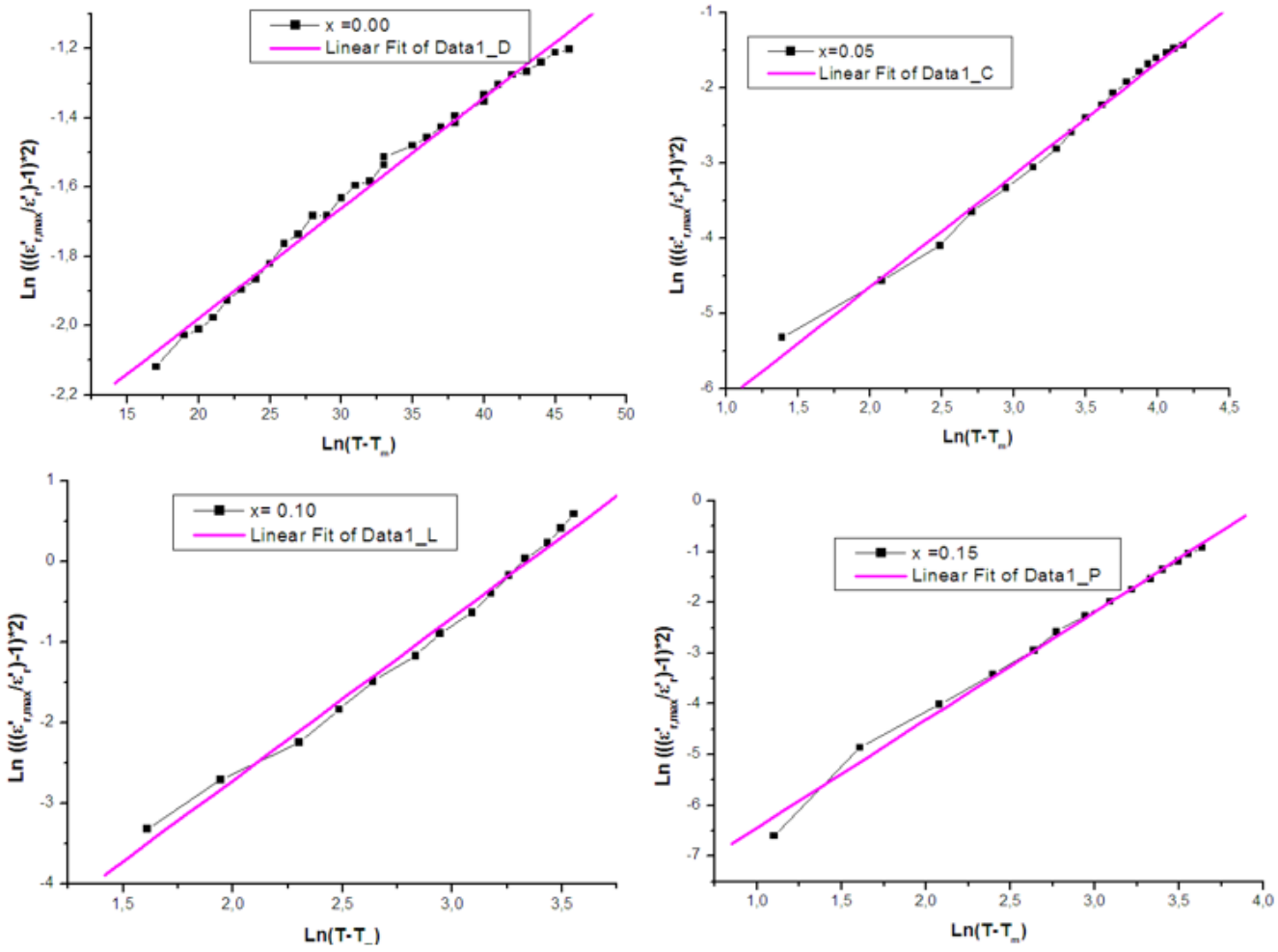

Figure 9

The plot of Ln(1/ε'r - 1/ε'r,max) as a function of Ln(T-Tm) at 5 KHz at TR-O for Ba1-xBixTi0.80Fe0.20O3 ceramics for x= 0.00, 0.05, 0.10 and 0.15.

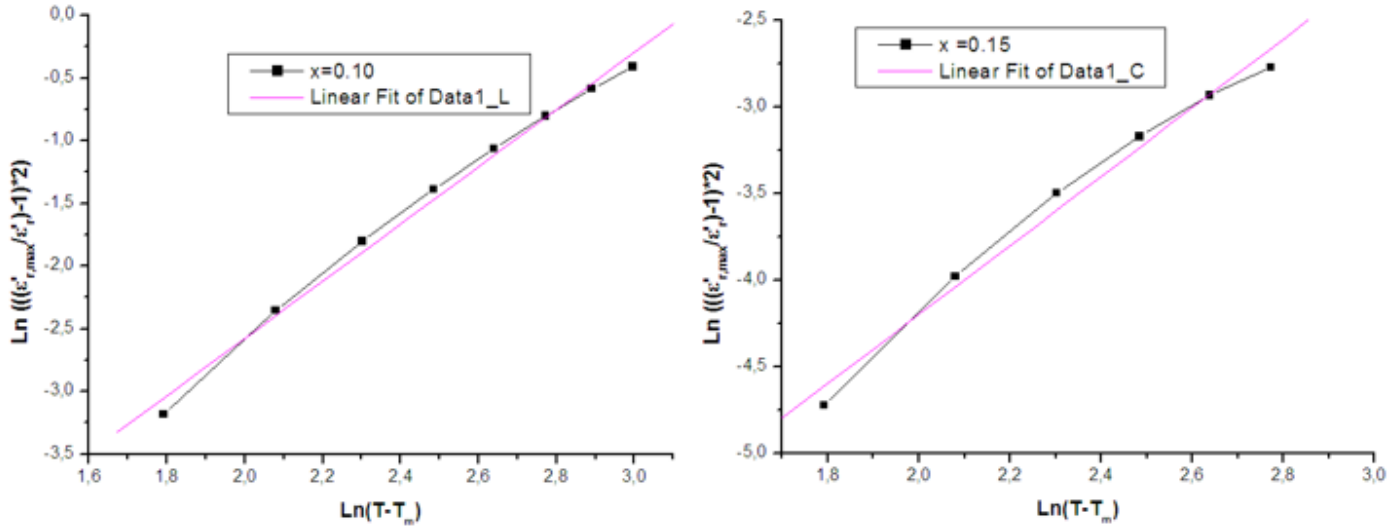

Figure 10

The plot of Ln(1/ε'r - 1/ε'r,max) as a function of Ln(T-Tm) at 5 KHz at TR-O for Ba1-xBixTi0.80Fe0.20O3 ceramics for x= 0.10 and 0.15.

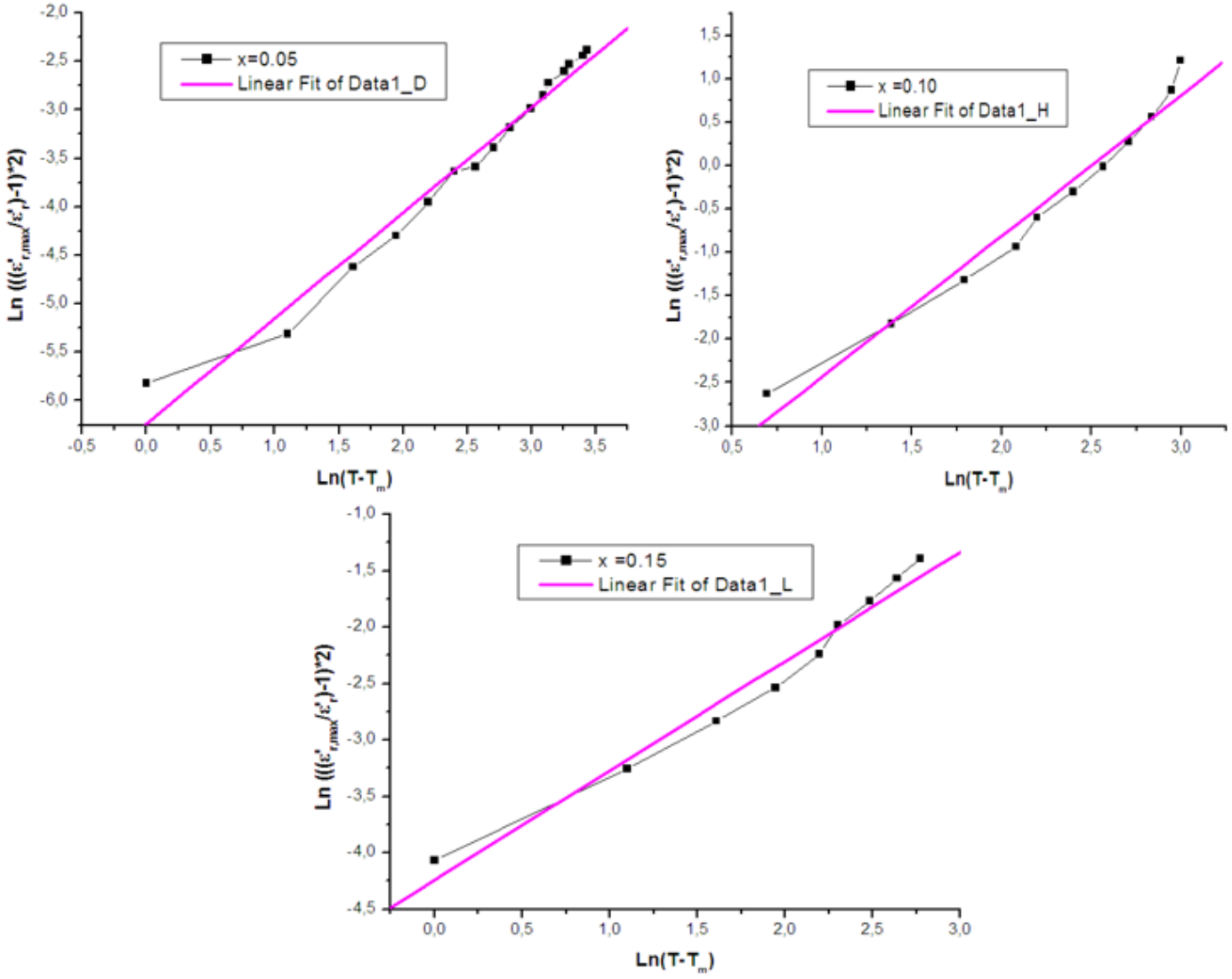

Figure 11

The plot of Ln(1/ε'r - 1/ε'r,max) as a function of Ln(T-Tm) at 5 KHz at Tm for Ba1-xBixTi0.80Fe0.20O3 ceramics for x= 0.05, 0.10 and 0.15.

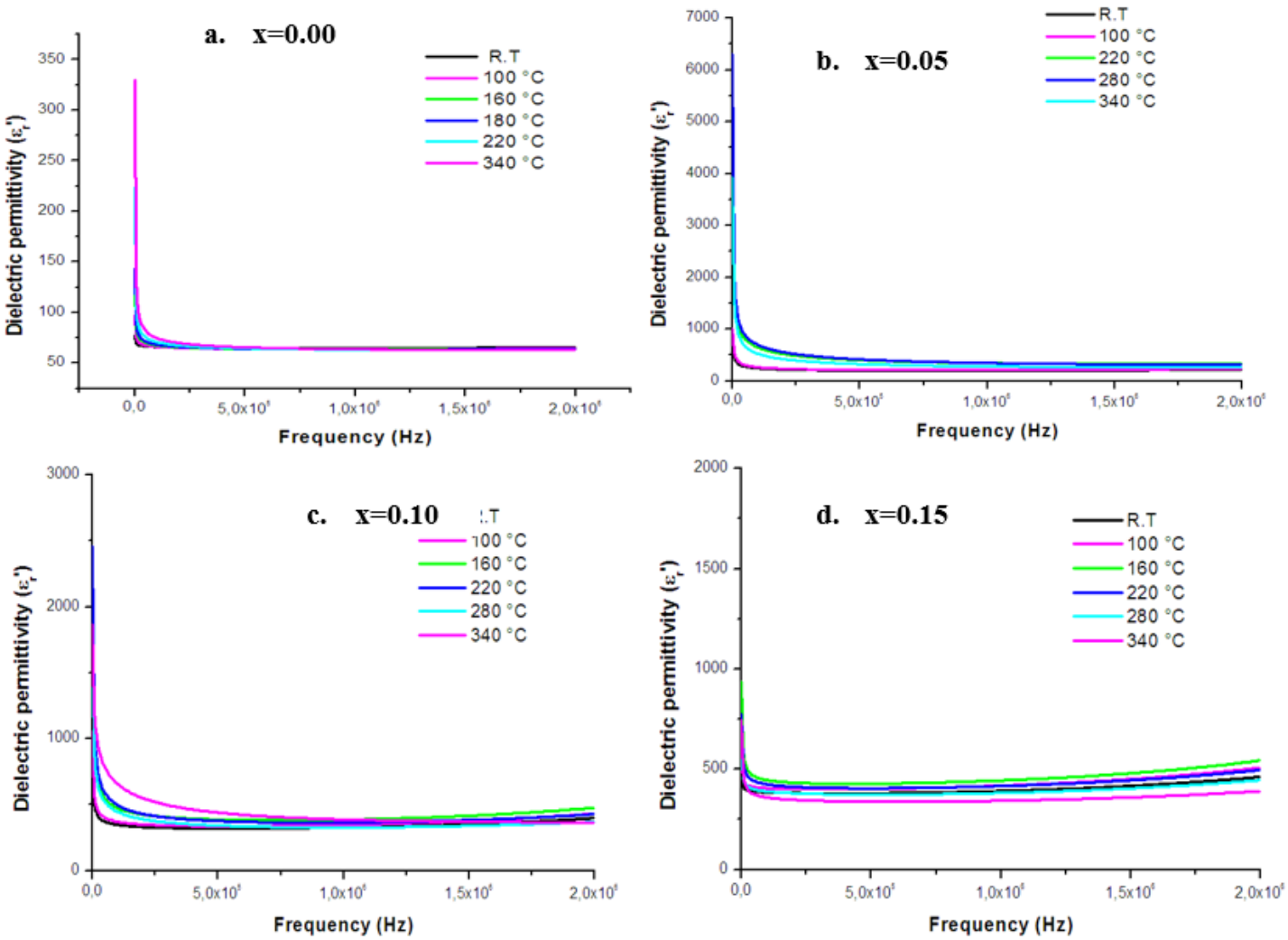

Figure 12

Fig.9. Dielectric constant dependent frequency at different frequencies of Ba1-xBixTi0.80Fe0.20O3 ceramics for a. x= 0.00, b. 0.05, c. 0.10 and d. 0.15.

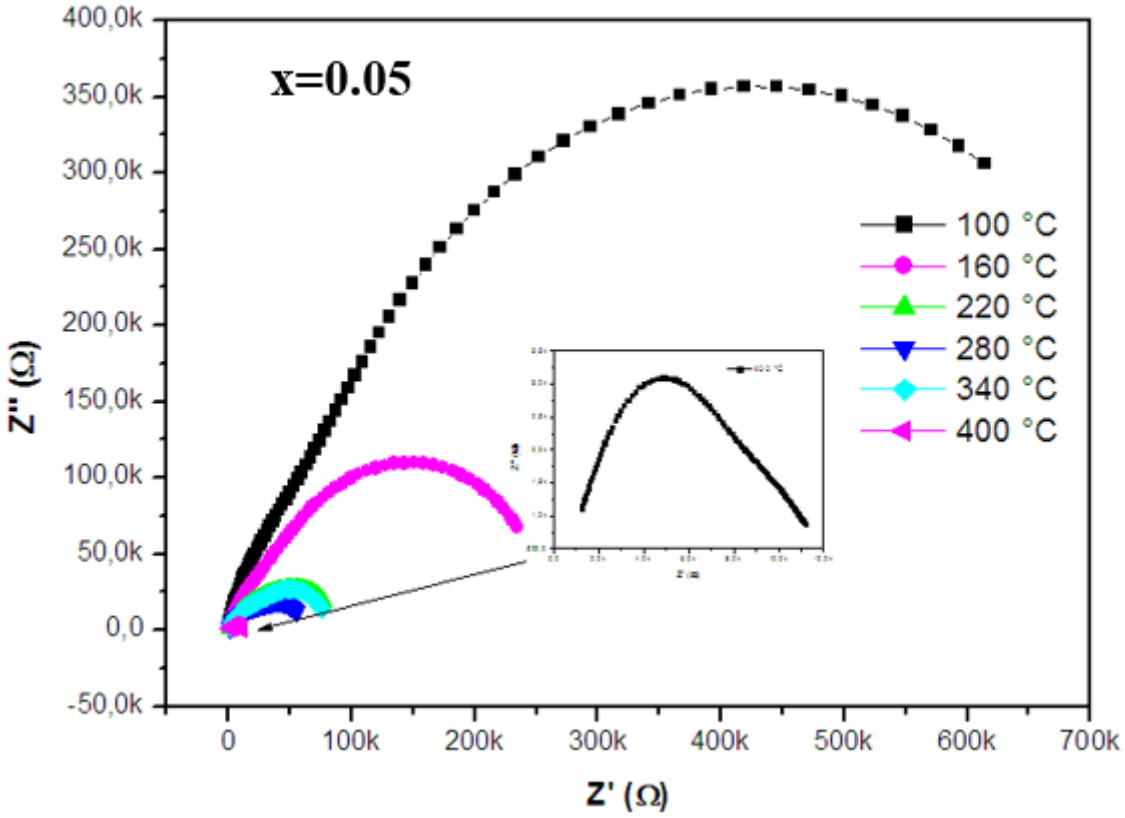

Figure 13

Fig.10. Complex impedance spectrum of Ba1-xBixTi0.80Fe0.20O3 ceramic at x= 0.05 at different temperature.

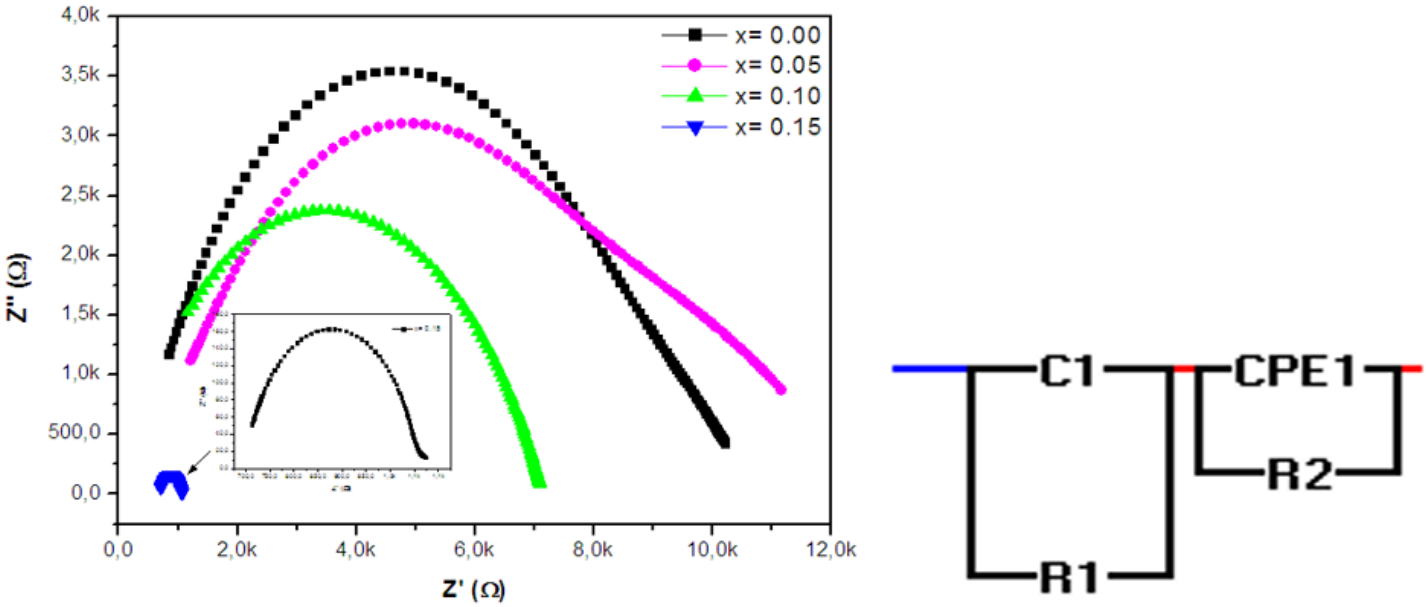

Figure 14

Fig.11. Complex impedance spectrum of Ba1-xBixTi0.80Fe0.20O3 ceramics for x= 0.00, 0.05, 0.10 and 0.15 measured at 400 °C.

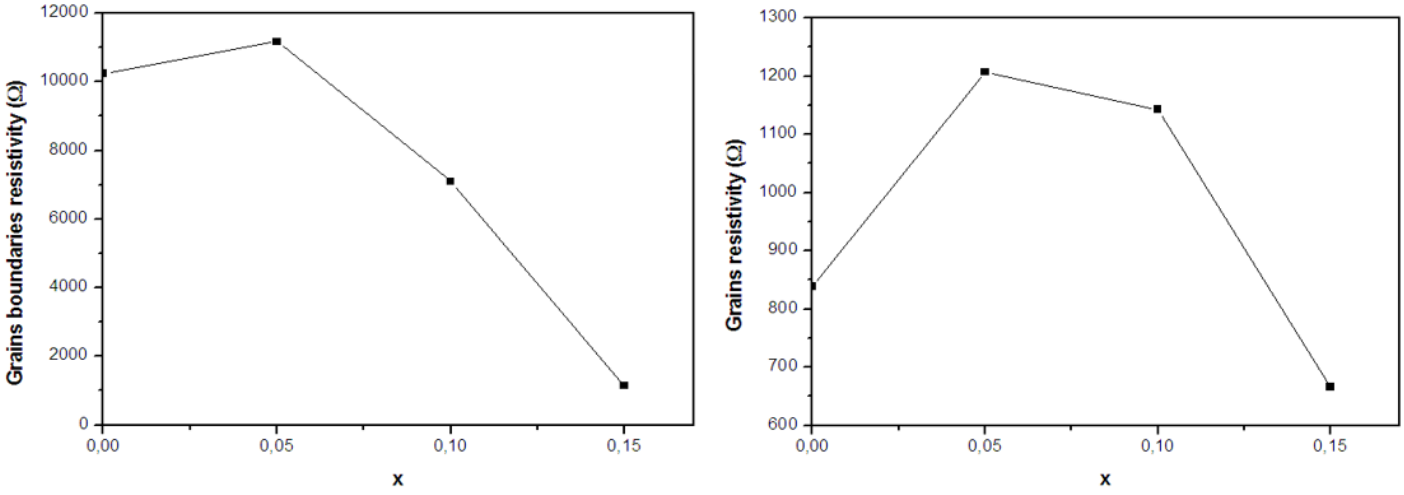

Figure 15

Fig.12. Evolution of grains and grains boundaries resistivity of Ba1-xBixTi0.80Fe0.20O3 ceramics for x= 0.00, 0.05, 0.10 and 0.15 measured at 400 °.